

# RSC Advances



This is an *Accepted Manuscript*, which has been through the Royal Society of Chemistry peer review process and has been accepted for publication.

*Accepted Manuscripts* are published online shortly after acceptance, before technical editing, formatting and proof reading. Using this free service, authors can make their results available to the community, in citable form, before we publish the edited article. This *Accepted Manuscript* will be replaced by the edited, formatted and paginated article as soon as this is available.

You can find more information about *Accepted Manuscripts* in the [Information for Authors](#).

Please note that technical editing may introduce minor changes to the text and/or graphics, which may alter content. The journal's standard [Terms & Conditions](#) and the [Ethical guidelines](#) still apply. In no event shall the Royal Society of Chemistry be held responsible for any errors or omissions in this *Accepted Manuscript* or any consequences arising from the use of any information it contains.

**Improved Electrochemical and Photovoltaic performance of dye sensitized solar cell based on PEO/ PVDF-HFP/Silane modified TiO<sub>2</sub> electrolytes and MWCNT/Nafion<sup>®</sup> counter electrode**

**K. Prabakaran, Smita Mohanty\* and Sanjay Kumar Nayak**

Laboratory for Advanced Research in Polymeric Materials, Central Institute of Plastics

Engineering & Technology, Bhubaneswar, Odisha, India-751 024.

**\* Dr. Smita Mohanty**

Laboratory for Advanced Research in Polymeric Materials (LARPM)

Central Institute of Plastics Engineering and Technology,

Bhubaneswar-751 024

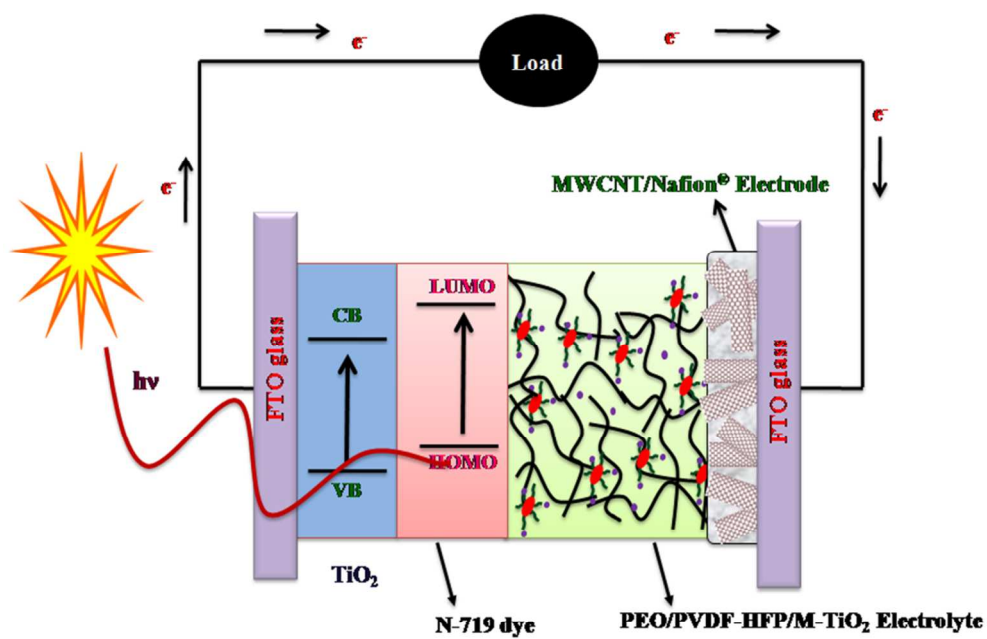
Odisha, India.

Email: papers.journal@gmail.com

Phone No: 0674 2742852

Fax No: 0674 2740463

## Graphical Abstract



Solid State Dye sensitized solar cells based on PEO/PVDF-HFP/M-TiO<sub>2</sub>

**ABSTRACT**

Polymer blend electrolyte membrane was prepared for dye sensitized solar cells based on poly ethylene oxide and polyvinylidene fluoride-co-hexafluoropropylene (PVDF-HFP) filled with surface modified Titanium dioxide (M-TiO<sub>2</sub>) nanofillers. The surface of TiO<sub>2</sub> was modified using Aminopropyltrimethoxysilane. The electrochemical studies indicated that the addition of surface modified nanoparticles increase the ionic conductivity up to  $7.21 \times 10^{-4}$  S/cm for 7 wt%, whereas the ionic conductivity about  $8.14 \times 10^{-5}$  S/cm with the addition of unmodified counterpart as the filler into the PEO/PVDF-HFP blend system. In addition to this ionic mobility, charge carrier concentration, ion diffusion coefficient also found to increase with the addition of surface modified TiO<sub>2</sub> nanoparticles. Wide angle X-ray diffraction (WAXD) results showed the change in the crystalline phase of PEO/PVDF-HFP blend electrolyte with the addition of M-TiO<sub>2</sub>. The influence of the TiO<sub>2</sub> nanoparticles surface functionality on the degree of crystallinity of the polymer matrix was analyzed using differential scanning Calorimetry (DSC). Thermo mechanical behavior of the composite membranes was studied by dynamical mechanical Analysis (DMA). The thermo gravimetric investigations (TGA) of membranes indicated the thermal degradation temperatures of hybrid nanocomposites were enhanced upon the addition of nanosized inorganic fillers. The morphological characterizations were carried out by atomic force microscopy (AFM). The solid state dye sensitized solar cell has been fabricated by using silane modified TiO<sub>2</sub>/PEO/PVDF-HFP polymer nanocomposites electrolyte, multiwalled carbon nanotube (MWCNT)/Nafion<sup>®</sup> as counter electrode. The photovoltaic characteristics of constructed cells showed an enhancement of open circuit voltage ( $V_{oc}$ ) from 0.62 to 0.71 V and the best efficiency achieved about 2.84%. The enhancement of DSSC was further confirmed by electrochemical impedance spectra (EIS) spectra studies for lowest Warburg resistance ( $R_{diff}$ ).

**Keywords:** PEO/PVDF-HFP, EIS, DMA, MWCNT.

## 1. INTRODUCTION

Since 1991, a great discovery of dye sensitized solar cells (DSSC) by Gratzel has been attracting much attention because of its simple structure and low cost.<sup>1</sup> The typical structure of DSSC consists of two sandwiched conducting glass plates; one is coated with a wide band gap and mesoporous semiconducting layer of nanoparticles with a self-assembled monolayer of chemisorbed dye molecules is called as photo anode filled with an electrolyte for dye regeneration and Pt, Carbon, *etc*, coated another glass plate used as counter electrode.<sup>2</sup> The remarkable improvements have been achieved in the performance and the maximum efficiency of DSSC about 11 % has been reported by using liquid electrolyte and ruthenium dyes.<sup>3</sup> However, the major drawback of these solar cells is leakage of solvent and high temperature instability, dye desorption, electrode corrosion which causes the sealing and performance degradation of DSSCs.<sup>4</sup> To overcome these problem for commercial exploitation of DSSC; many efforts have been focusing on long term stability and to replace the liquid electrolyte medium by using solid p type inorganic materials, organic hole conductors, ionic liquids and gel/solid polymer electrolytes.<sup>5-8</sup> Among these alternatives, solid polymer electrolytes (SPEs) have received considerable attention, because of their outstanding performance in solid-state batteries, electrochromic devices, fuel cell and photoelectrochemical cells were extensively studied.<sup>9-11</sup> Among the polymers used in electrochemical device applications, PEO and PVDF-HFP are the most searched host materials due to their unique characteristics. The presence of fluorine that has a relatively smallest ionic radius and high electro negativity PVDF-HFP is expected to improve the ionic transport and reduce the recombination rate at the semiconductor-polymer electrolyte interface in DSSC.<sup>12</sup> And also PVDF-HFP is known to be photochemically stable even in the presence of TiO<sub>2</sub> and Pt, which makes it is a suitable electrolyte in DSSC for long term stability applications.<sup>13</sup> It has a high dielectric constant of  $\epsilon = 8.4$  which can help in

better dissociation of ionic salts.<sup>14</sup> The crystalline phase vinylidene fluoride (VDF) units provide excellent chemical stability and mechanical strength and amorphous hexa fluoropropylene (HFP) units increase its plasticity and enhance ionic conductivity. Even in the presence of HFP, the ionic conductivity of PVDF-HFP is about  $10^{-8}$ - $10^{-10}$  S/cm. Utilization of PEO based electrolytes has improved the performance and stability, which is originated from the existence of more number of channels between electrodes to maintain the liquid like nature for fast ion transport. The  $\text{CF}_2$  group is present in PVDF-HFP structure can give a better compatibility while blending with other polymer particularly PEO due to the strong interaction to C-O-C.<sup>15</sup>

The additional incorporations of nanoparticles into the polymer matrix can reduce the crystallinity of the polymer, reducing recombination rate at electrode/ electrolyte interface,<sup>16</sup> gives a three dimensional, mechanically stable and create a porous network structure. The anions in the present structure (iodide/tri iodide) can easily move into the porous structures. In addition, highly charged surfaces of the nanoparticles add up as the conductive path.<sup>17</sup>

Variety of nanoparticles such as  $\text{SiO}_2$ ,  $\text{ZnO}$ ,  $\text{SnO}_2$ ,  $\text{TiO}_2$ ,  $\text{ZrO}_2$ , *etc* have been employed as fillers in polymer nanocomposite electrolytes for dye sensitized solar cell applications.<sup>18-24</sup> Among them  $\text{SiO}_2$  and  $\text{TiO}_2$  nanoparticles were more investigated fillers for solid state DSSC electrolyte applications. The interfacial resistance of each interface (Photo anode/electrolyte/counter electrode) in DSSC plays main role in the photo conversion efficiency. When  $\text{TiO}_2$  is added into PEO/PVDF-HFP electrolytes, the compatibility between polymer electrolytes and photo anode based on  $\text{TiO}_2$  nanoparticles is increased.<sup>25</sup> Hence, photocurrent and efficiency will be enhanced. Recently, comparative studies of  $\text{TiO}_2$  and  $\text{SiO}_2$  within the polymer electrolyte have been reported by Tiautit et al. It is reported that the charge transfer resistance and diffusion resistance of  $\text{TiO}_2$  incorporated electrolyte is very lesser than  $\text{SiO}_2$ .<sup>19</sup>

Generally, in polymer nanocomposites electrolytes the high surface energy of nanoparticles restricts the uniform dispersion of the fillers within the matrix. This will impede to achieve desired ionic transport behaviour for DSSC applications. Surface modification of fillers has been identified as a feasible method reduces the surface energy of nanoparticles while improving its dispersion to achieve required performance characteristics. Many results have been reported on surface modifications of nanoparticles employing organic molecules includes silanes, phosphonic acid, ethylene diamine for majorly dielectric applications. Among the modifiers silane coupling agents have the structure of  $(XO)_3SiY$ , where XO is a hydrolysable alkoxy group which can be ethoxy ( $OC_2H_5$ ) or methoxy ( $OCH_3$ ) and Y is an organo functional group. The formation of silane functional groups is based on the condensation reactions between silanols and the hydroxyl group on metal oxide surface.<sup>26</sup> Recently, our group has investigated the effect of APS silane modified  $TiO_2$  on the electrical properties of PVDF-HFP composites and also it was found that reduction in crystallinity, glass transition temperature as well as uniform distribution of  $TiO_2$  achieved.<sup>27</sup> Because the amine ( $-NH_2$ ) group of APS is expected to react with C–F groups of PVDF through the formation of hydrogen bonds due to the possible formation of F–H bonds. Hence, it can be enhanced the compatibility between nanofillers and polymers. Even the strategy of surface modified of  $TiO_2$  nanoparticles reinforced PEO/PVDF-HFP nanocomposites has seldom been studied on electrochemical properties. In addition the surface modifications of  $TiO_2$  by aminopropyl trimethoxy silane (APS) is widely accepted technique for poly urethane based coating applications, because this forms hydrated oxides and capture the formation of hydroxyl radicals. Hence it will help to minimize the photo catalytic activity of pure  $TiO_2$  nanoparticles.<sup>28</sup>

Furthermore, counter electrode plays the important role in high efficient dye sensitized solar cells. Generally, thin layer of platinum (Pt) coated transparent conducting oxide substrate is widely used as counter electrode. But it is well known that Pt is expensive and issues of

corrosion in tri-iodide solution restrict the practical viability. To consider commercialization of a DSSC, Pt should be replaced with other cheaper materials like conducting polymers (CPs)/ carbon based nano materials.

In this work, the aforesaid key issues of DSSCs have been taken into account to develop a solid state dye sensitized solar cells. At first mainly, we studied the effect of surface modified TiO<sub>2</sub> nanoparticles on PEO/PVDF-HFP on structural, thermal, morphological, optical, thermo mechanical and electrical properties. Then, MWCNT/Nafion® composite was explored as a counter electrode and photovoltaic performance of solid state dye sensitized solar cells were studied

## 2. Experimental procedure

### 2.1. Materials

Poly (vinylidene fluoride-co-hexafluoropropylene) (PVdF-HFP, Kynar flex 2801) was supplied by Arkema (India), poly ethylene oxide (PEO) (Mw  $5 \times 10^6$ ), aminopropyltrimethoxysilane (APS), nafion117 solution, Triton X-100 and chloroplatinic acid hexahydrate (H<sub>2</sub>PtCl<sub>6</sub>) purchased from M/S Sigma Aldrich, multiwalled carbon nanotubes (MWCNT) of >98% purity and diameter of 80–100 nm was purchased from M/s Nanoshel, Intelligent Materials Pvt. Ltd, India, bis(tetrabutylammonium)dihydrogen bis(isothiocyanato) bis (2,2'-bipyridyl-4,4'-dicarboxylato) ruthenium(II) (N719) dye was purchased from Solaronix, Switzerland. anhydrous dimethyl formamide (DMF), ethanol, anhydrous lithium iodide (LiI), iodine (I<sub>2</sub>), Lithium perchlorate (LiClO<sub>4</sub>), acetylacetone, n-butanol, isopropyl alcohol were purchased from Himedia India and FTO glass plate (Rs<10 ohm/cm<sup>2</sup>) were purchased from supplied by M/s. Shilpa Enterprises, India. TiO<sub>2</sub> nanoparticles (P25), 25-30 nm, Degussa, AG Germany were dried at 80°C for 10 hrs in a vacuum oven prior to use.

### 2.3. Preparation of Polymer blend nanocomposite Electrolyte

Surface of TiO<sub>2</sub> nanoparticles were modified by using APS as reported in our previous literature.<sup>23</sup> The hybrid nanocomposite polymer electrolyte membranes were prepared using solvent-casting technique, described as follows. An optimized composition of (6:4 wt%) of poly (vinylidene fluoride-co-hexafluoropropylene) (PVDF-HFP) and poly ethylene oxide (PEO) is dissolved in DMF at 80°C. Then, predried surface modified TiO<sub>2</sub> was slowly introduced with different weight percent (1-10 wt.%). The mixture was thoroughly mixed under continuous stirring about 8 h. Subsequently, the mixtures were poured in glass petri-dishes and the solvent was allowed to evaporate. Finally, the dimensionally stable hybrid nanocomposite polymer electrolyte membranes were obtained. The formulation of surface modified TiO<sub>2</sub> and was optimized by ionic conductivity as 7 wt%. For comparison purpose optimized percentage of unmodified TiO<sub>2</sub> nanoparticles was also separately incorporated into the blend matrix and the polymer electrolytes were obtained by the same procedure. Hereafter, APS treated TiO<sub>2</sub> and untreated TiO<sub>2</sub> nanoparticles incorporated blends are named as PEO/PVDF-HFP/M-TiO<sub>2</sub> and PEO/PVDF-HFP/U-TiO<sub>2</sub> respectively in the forthcoming sections.

### 2.4. Fourier Transform Infrared Spectroscopy (FTIR):

Fourier transform infrared (FTIR) spectra of the PEO/PVDF-HFP electrolyte samples were performed on a NICOLET 6700, USA FTIR spectrometer from 4000 to 400 cm<sup>-1</sup> with a scan rate of 5cm<sup>-1</sup>sec.

### 2.5. Wide Angle X-ray Diffraction (WAXD)

X-ray analysis was conducted in Shimadzu X-ray diffractometer, Japan using CuK<sub>α</sub> (1.514Å) at a scanning rate of 5° /min over a 2θ interval from 2° to 80°.

### 2.6. Thermal Characterization

DSC of the polymer composite electrolyte membranes was carried out using DSC, Q20, M/s TA Instruments (USA) equipment. Samples of  $\leq 7$  mg was heated from  $-60^{\circ}$  to  $200^{\circ}$  C, at the heating rate  $5^{\circ}\text{C}/\text{min}$  under nitrogen atmosphere.

Thermal stability of the membranes was evaluated using thermo gravimetric analyzer (TGA, Q50, TA Instruments USA). Samples of about 7 mg were heated from room temperature to  $800^{\circ}\text{C}$  at a linear heating rate of  $10^{\circ}\text{C}/\text{min}$  under  $\text{N}_2$  flow (20 ml /min).

### **2.12. Dynamic mechanical Analysis (DMA)**

Dynamic mechanical properties were measured using dynamic mechanical analyzer (M/s. TA Instruments, USA), operating in the tension film mode at an oscillation frequency of 1.0 Hz. The samples were heated from  $-60^{\circ}\text{C}$  to  $120^{\circ}\text{C}$  at a heating rate of  $10^{\circ}\text{C}$  per min.

### **2.8. UV-VIS Spectra Studies**

The tri-iodide and iodide absorption spectra of PVDF-HFP and its composite samples were performed by UV-VIS spectrophotometer (UV-2450, M/s Shimadzu, Japan) in the range of 200 nm to 600 nm.

### **2.9. Surface characterization**

Surface characterization for the PEO/PVDF-HFP blend nanocomposites electrolytes was carried out in PARK XE-100, South Korea, using non-contact mode.

### **2.11. Electrochemical Impedance Spectroscopy (EIS)**

The ionic conductivity measurements were carried out from electrochemical impedance spectroscopy technique by using WonATech-ZiveSP2 (Korea) electrochemical workstation. A perturbation of sinusoidal voltage signal of 10 mV was applied over a frequency range of 1 mHz-1MHz at room temperature. The impedance plots were fitted using Zview2-smart manager software. The samples were sandwiched between circular metal blocking electrodes with a

diameter of 10 mm. The thickness of polymer nanocomposite electrolyte membranes was varied from 40 to 200 microns measured by thickness gauge.

### 2.13. Preparation of TiO<sub>2</sub> Photo anode

0.1g of TiO<sub>2</sub> nanoparticles were taken in a mortar, pestle and ground for 10 minutes with the sequential addition of 0.2 ml of distilled water and 0.02 ml of acetyl acetone to achieve a viscous colloidal form. Finally, 0.34 ml of distilled water and 20  $\mu$ l of triton-X 100 were slowly added with continuous mixing to get uniform paste. To remove the organic impurities and other contaminants, the FTO glasses (1.5cm x 1.5 cm dimensions), with a sheet resistance of  $R_{sh} < 10$  ohm/cm<sup>2</sup>, were introduced into ultrasonication and thoroughly cleaned in acetone, ethanol and distilled water, for 15 min in each steps. The colloidal paste was uniformly spread over the area of 0.5 cm<sup>2</sup> area on the FTO coated glass substrate ( $R_{sh} < 10$  ohm/cm<sup>2</sup>) by doctor blade technique. The slide was kept for 5 min in atmospheric condition for drying. After drying the TiO<sub>2</sub> film was calcined at 450° C for 30 min and cooled to 80°C in an oven. Subsequently, the films were immersed in 0.3 mM N-719 dye in acetonitrile and n-butanol (1:1 volume ratio) solution for 24 h.

### 2.14. Preparation of counter electrode.

FTO glasses (1.5cm x 1.5 cm dimensions) were cleaned with same procedure mentioned in the above section. The different amount (0.5wt%, 1wt%, 1.5% and 2wt %) of MWCNT is dispersed in ethanol/Nafion<sup>®</sup> solution with the volume percentage of (90:10) %. The mixer was kept under ultrasonication for 3 hrs at room temperature. The viscous solution of MWCNT/Nafion<sup>®</sup> composite was coated on FTO glass plate drop casting. The MWCNT/Nafion<sup>®</sup> coated FTO sample were kept at 50°C in oven for 5 h. For comparison purpose platinum-coated (Pt) counter electrode has been prepared by spreading a drop of 5 mM

chloroplatinic acid hexahydrate ( $\text{H}_2\text{PtCl}_6$ ) in isopropyl alcohol on separate FTO substrate and calcinated it at  $450^\circ\text{C}$  for 15 min under air ambient.

### 2.15. Cyclic Voltammetry studies

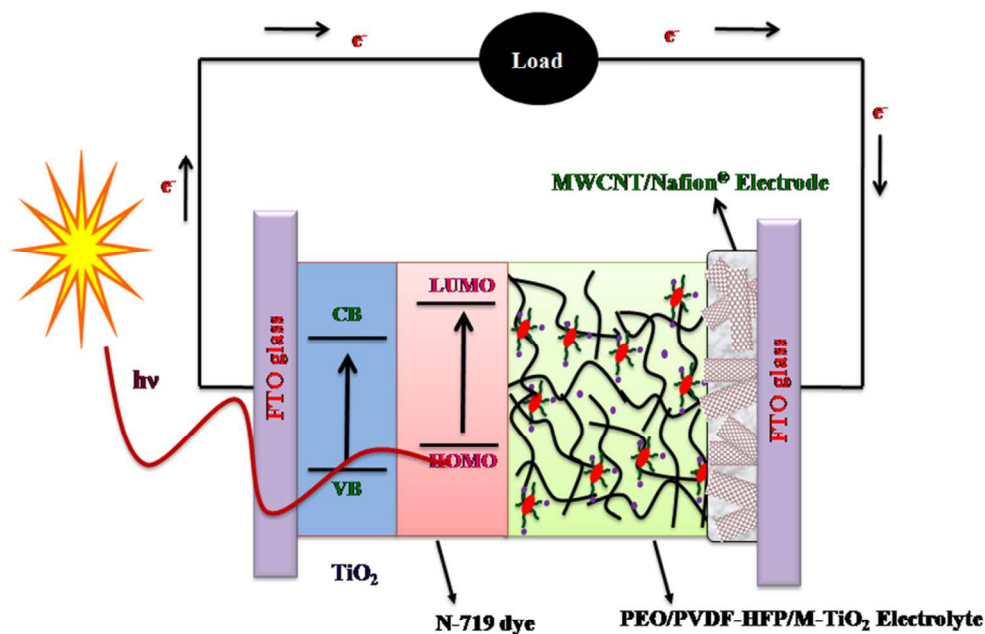
Cyclic voltammetry (CV) was performed to investigate electrocatalytic properties of the CEs. The CV was carried out with a three-electrode electrochemical system, by using an electrode of MWCNT/Nafion<sup>®</sup> composite as the working electrode, a Pt foil as the CE, and saturated calomel electrode as a reference electrode as the reference in an electrolyte solution (10.0 mM I, 1.0 mM  $\text{I}_2$ , and 0.1 M  $\text{LiClO}_4$  in acetonitrile). For comparison purpose as prepared platinum (Pt) counter electrode also employed as a working electrode. All the samples were performed with 10 mV/s scan rate.

### 2.16. Construction of Solid state dye sensitized solar cells (SSDSSC)

The PEO/PVDF-HFP/M-TiO<sub>2</sub> polymer composite electrolyte solutions were casted onto the dye adsorbed TiO<sub>2</sub> photo anode by drop casting. Then the MWCNT/Nafion<sup>®</sup> coated FTO glass plate is compressed on photo anode without any short circuit. Finally, sandwich type SSDSSC configuration was clamped with binder clip and kept in the oven at  $50^\circ\text{C}$  for 12 hrs to remove the residual solvent completely. The schematic diagram of DSSC is shown in **scheme. 1**.

### 2.17. Characterization of SSDSSC

The photovoltaic performance of the DSSC is studied using Oriel Class-A Simulator (M-91900 A, Newport) with Xenon lamp as a light source having a intensity of  $100\text{mW}/\text{cm}^2$ . A computer controlled Auto lab PGSTAT302N electrochemical workstation was used for J-V measurements. The active area of the cell was  $0.5\text{ cm}^2$ . To analyze the internal resistance of DSSC, EIS measurements were carried out by WonATech-ZiveSP2 (Korea) electrochemical workstation with a signal frequency range from 1 mHz-1MHz under the illumination of  $100\text{ mWcm}^{-2}$ .



Scheme.1. Solid State sensitized solar cells

### 3. Results and Discussion.

#### 3.1. FTIR studies

FTIR spectra of the PEO/PVDF-HFP, PEO/PVDF-HFP/U-TiO<sub>2</sub>, PEO/PVDF-HFP /M-TiO<sub>2</sub> blend electrolyte, membranes are shown in **Figure.1. (a-c)**. The IR spectra of the electrolyte membranes were characterized in the range of 4000-400 cm<sup>-1</sup> at room temperature. It is well-known that potassium iodide forms complexes with C-O-C in PEO and C-F in PVDF-HFP which results in decreasing the stretching vibration frequency of these groups in FTIR spectra.<sup>29</sup>

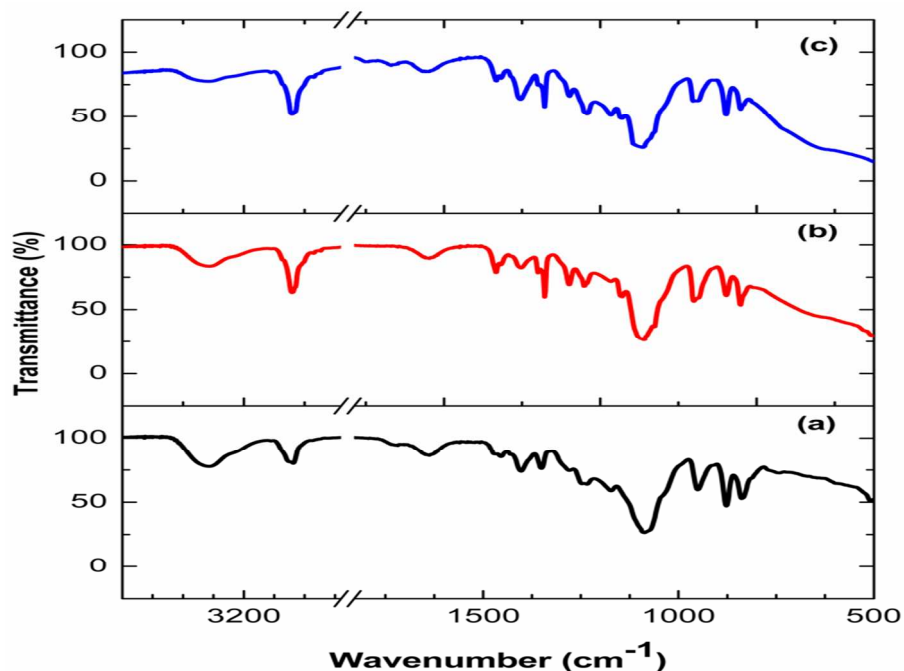


**Figure.1. FTIR spectra of electrolytes (a) PEO/PVDF-HFP (b) PVDF-HFP U-TiO<sub>2</sub> and (c) PEO/PVDF-HFP M-TiO<sub>2</sub>**

The stretching and bending modes of CH<sub>2</sub> in PEO is observed around 1470 and 1350 cm<sup>-1</sup>.<sup>30</sup> The deformed vibration of CH<sub>2</sub> groups appears at 1403 cm<sup>-1</sup>.<sup>31</sup> The characteristics peaks correspond to 1071 cm<sup>-1</sup>, 759 cm<sup>-1</sup> and 607 cm<sup>-1</sup> are primarily due to the crystalline form of PVDF-HFP, whereas the bands at 872 and 841 cm<sup>-1</sup> are assigned to amorphous phase of PVDF-HFP. The peaks observed in the frequencies 1280-1050 cm<sup>-1</sup> are denoted to -CF and -CF<sub>2</sub> stretching vibrations.<sup>32</sup> Another important characteristic of CH<sub>2</sub> symmetric and -CH<sub>2</sub> asymmetric peaks were observed at 1280 cm<sup>-1</sup> and 3018 cm<sup>-1</sup> respectively. The typical deformed vibrational frequency of CH<sub>2</sub> group was observed at 1400 cm<sup>-1</sup>. The vibrational peaks around 504 cm<sup>-1</sup> and 420 cm<sup>-1</sup> are assigned to bending and wagging frequencies of -CF<sub>2</sub>. The scissoring vibration of vinylidene was observed at 1404 cm<sup>-1</sup>. The peak at 880 cm<sup>-1</sup> corresponds to the vinylidene group of PVdF.<sup>33</sup> The strong absorption band around 1095 cm<sup>-1</sup> it is assigned to be main characteristics peak of non resolved anti-symmetric and symmetric stretching of C-O-C in polymer back bone chains of pure polycrystalline PEO it is shifted from 1119 cm<sup>-1</sup>. This red shift has observed due

to the formation of a transient cross-linking complex between the cations of the electrolyte salt and the ether oxygen of the PEO, so that the generated transition state will weaken the C-O-C stretching vibration and the crystallization of PEO will be decreased.<sup>34</sup>

The intensity of characteristics peak of PEO around  $1095\text{ cm}^{-1}$  and crystalline peak PVDF-HFP about  $1070\text{ cm}^{-1}$  were weakened in PEO/PVDF-HFP blend electrolyte system, which indicates the PVDF-HFP is well blended with PEO matrix. The peaks were broadened and intensity decreased with the addition of U-TiO<sub>2</sub> and M-TiO<sub>2</sub>. This may be due the reinforcement effect of nanoparticles on polymer matrix, it reduce the recrystallization. It suggests that the nanoparticles were significantly affecting the crystallinity of high molecular weight semi crystalline PEO/PVDF-HFP blend. The possible interactions can be explained in the forthcoming sections.

The broad band absorptions of -OH stretching should negligible in high average molecular weight PEO, but it observed in the range of frequency  $3600\text{-}3200\text{ cm}^{-1}$ . This is might be due to that large number of intermolecular and intramolecular hydrogen bonds is formed by the interactions of solvent and PEO/PVDF-HFP. In U-TiO<sub>2</sub> incorporated electrolyte membrane, water molecules on the surface of nanoparticles might be a reason of absorption in these regions. The intensity of -OH stretching was decreased in M-TiO<sub>2</sub> incorporated electrolyte membrane, which indicates the hydrolysis condensation reaction of APS molecules present on the TiO<sub>2</sub> nanoparticles

In PEO/PVDF-HFP/7%M-TiO<sub>2</sub> membrane, NH<sub>2</sub> group was observed at  $1600\text{ cm}^{-1}$  which is shifted to the lower wave number around  $1580\text{ cm}^{-1}$ . This indicates the fact that more number ions coordination with -NH<sub>2</sub>. The new interaction of salt-TiO<sub>2</sub> and TiO<sub>2</sub>-polymer in the FTIR spectra of PEO/PVDF-HFP blend nanocomposite electrolyte membranes can be expected to improve the ionic conductivity of the system. The possible interactions of other characteristic peaks of APS such as Si-O-Si, C-N are not distinguishable as these peaks overlapped with the

major peaks of PEO/PVDF-HFP blend matrix. Hence, it could not be resolved from the major peaks of PEO/PVDF-HFP matrix and it can be explained in forthcoming sections.

### 3.2. Wide angle X-ray diffraction (WAXD)

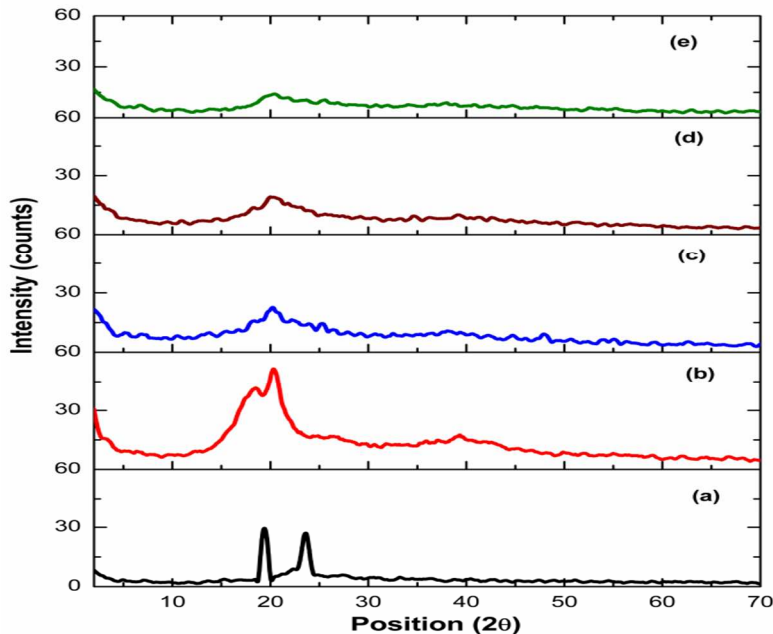


**Figure. 2.** X-ray diffraction study of (a) PEO, (b) PVDF-HFP (b) PEO/PVDF-HFP (c) PEO/PVDF-HFP/U-TiO<sub>2</sub> and (d) PEO/PVDF-HFP / M-TiO<sub>2</sub> composite electrolyte membranes

**Figure.2.** (a-e) shows the WAXD pattern of PEO, PVDF-HFP, PEO/PVDF-HFP blend and its nanocomposite electrolyte membranes. The diffraction peaks at 19.36° 23.52° and 18.4°, 20.3°, 26.9° were observed that the characteristic peaks of crystalline phase of PEO and PVDF-HFP respectively in Fig. (2a & b).<sup>35, 36</sup> The peaks of pristine materials are significantly reduced in PEO/PVDF-HFP blend electrolyte, which indicates that the PEO is properly blended with PVDF-HFP and the crystallization of PEO is restricted while blended with PVDF-HFP. These diffraction peaks are slightly shifted towards higher angle side and broadening with decreased intensity in blend nanocomposite electrolytes. In all the cases, there is no additional peaks were

observed for lithium iodide (LI) and  $I_2$ , it suggests that the electrolyte salts were completely dissolved in polymer blend system.

In the case of PEO/PVDF-HFP blend nanocomposite electrolytes in Fig (d-e),  $TiO_2$  nanoparticles disturb the crystalline region and decrease the crystalline phase of PEO/PVDF-HFP blend than pure blend (**Fig.2c**). This behavior is due to large surface area of  $TiO_2$  nanoparticles, which inhibit the recrystallization of PEO/PVDF-HFP host. The addition of  $TiO_2$  nanoparticles could lead to a decrease in the intermolecular interaction between polymer chains hence increased the amorphicity.<sup>37</sup> These observations suggest that M- $TiO_2$  incorporated PVDF-HFP host undergoes more structural reorganization. This amorphous nature may lead to higher ionic conductivity which is generally observed in amorphous polymer electrolytes with flexible backbone.

### 3.3. Surface morphology of the electrolyte membranes using AFM

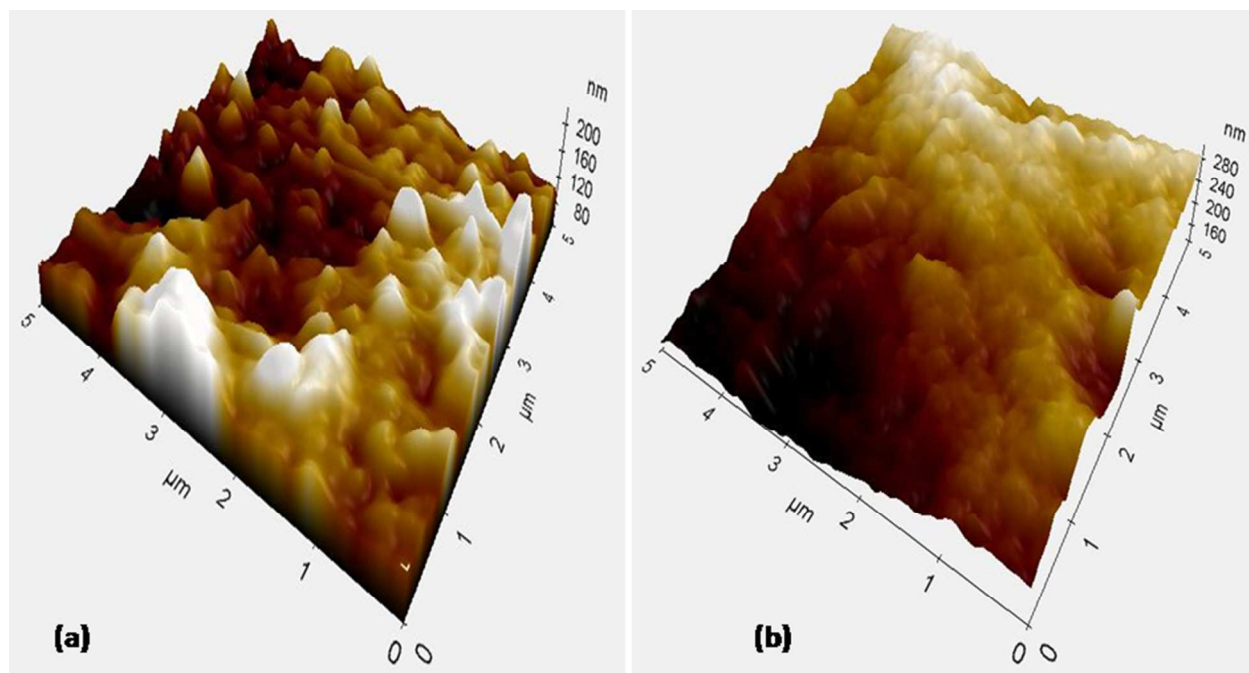
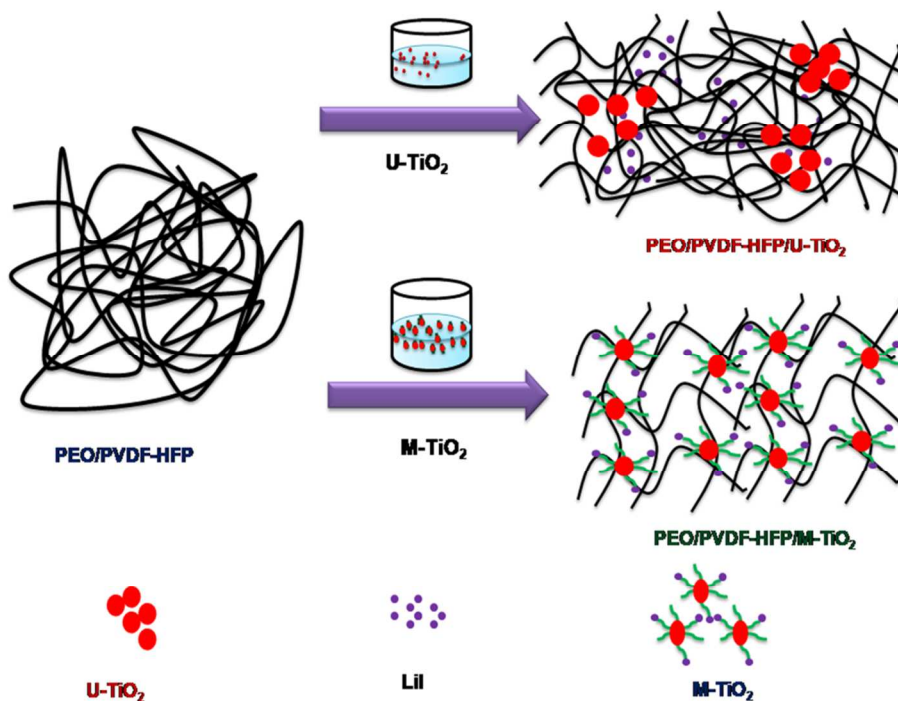


**Fig.3.** Surface morphology of (a) PEO/PVDF-HFP/ U- $TiO_2$  and (b) PEO/PVDF-HFP/M- $TiO_2$  electrolytes

Three dimensional topographical images of PEO/PVDF-HFP blend nanocomposite electrolyte membranes are presented in **Fig.3**. The PEO/PVDF-HFP/U-TiO<sub>2</sub> electrolyte shows morphology of rough surface and composed of spherical grains with the size of 200-300 nm. This is mainly due to the high surface energy of unmodified TiO<sub>2</sub> nanoparticles cause the agglomeration via particle-particle interaction among the TiO<sub>2</sub> nanoparticles. But, in the case of surface modified TiO<sub>2</sub> (M-TiO<sub>2</sub>) incorporated blend electrolytes showed comparatively smoother surface which indicates that M-TiO<sub>2</sub> particles are uniform distributed within the matrix. And also the smoother surface pointed out that more amorphous in nature than other. This behavior can be expected to improve ion transport properties polymer electrolytes. The possibility of surface modified TiO<sub>2</sub> nanoparticles dispersion and complexation in polymer matrix is shown **scheme-2**



**Scheme. 2. Dispersion of nanoparticles in PEO/PVDF-HFP blends**

### 3.4. Differential Scanning Calorimetry (DSC)

DSC thermograms of pure PEO, PVDF-HFP, PEO/PVDF-HFP and PEO/PVDF-HFP nanocomposite electrolyte membranes in wide range of temperature  $-60^{\circ}\text{C}$  to  $200^{\circ}\text{C}$  were shown in **Fig.s1. (a-e)** †. From the DSC thermograms, the glass transition temperature ( $T_g$ ), the melting temperatures of PEO ( $T_{m1}$ ), PVdF-HFP ( $T_{m2}$ ), melting enthalpy of PEO ( $\Delta H_{m1}$ ) PVDF-HFP ( $\Delta H_{m2}$ ) were determined. Here,  $T_m$  was obtained as the peak of the melting endothermic, and  $T_g$  as the inflection point. The glass transition temperature ( $T_g$ ) is an important parameter of amorphous phase for the flexibility of polymers at room temperature. The  $T_g$  of pure PEO and PVDF-HFP electrolytes is about  $-41.8^{\circ}\text{C}$  and  $-21.5^{\circ}\text{C}$  respectively.

When PEO is blended with PVDF-HFP, it shows a single glass transition temperature, which indicates that the all blend nanocomposites are miscible with homogenous phase in the blend electrolyte systems in **Fig.s1. (c-e)**†. Similar results have observed by J.Zhang et al.<sup>38</sup> The decreasing of  $T_g$  about  $-23.3^{\circ}\text{C}$  for PEO/PVDF-HFP electrolytes membranes than the pristine PVDF-HFP electrolyte is may be due to the addition of PEO host, which has softened the rigid segment of main matrix. The further addition of U-TiO<sub>2</sub> and M-TiO<sub>2</sub> nanoparticles were marginally reduced the glass transition temperature ( $T_g$ ). The incorporated nanoparticles are acting as the solid plasticizers and significantly it reduces the cohesive forces between the long range polymer chains of high molecular weight polymers. Hence, it increases the segmental motion/local chain flexibility, thereby reducing the  $T_g$  of the polymer blends. This in turn helps easy migration of the polymer chain which contributes in enhancing the ionic conductivity in the membrane. In f **Fig.s1 (b)** † there are few small peaks observed in between the glass transition temperature and melting which is probably due to crystal phase transition of ferroelectric to paraelectric phase in PVDF copolymer called as Curie temperature.<sup>39</sup> The endothermic sharp

peak with melting temperature ( $T_m$ ) of PEO and PVdF-HFP were observed around 60°C and 147°C respectively.

It is necessary to study the crystallinity of PEO, even though the amount (4 wt %) of PEO is less than the main matrix PVdF-HFP (6 wt %) in PEO/PVdF-HFP blend and its composite system in the present work. Because, the crystallization temperature of PEO is nearby room temperature (50-60 °C) can restrict the ionic movement. The addition of PVdF-HFP and nanoparticles result in broadening of the melting peaks of PEO, which suggest that there is interruption on the crystallization of PEO and the increase in the free volume fraction. The relative percentage of crystallinity ( $\% \chi$ ) was calculated from the following equation (1)

$$\% \chi = \Delta H_m / \Delta H_m^0 \times 100\% \quad \text{----- (1)}$$

Where,  $\Delta H_m^0$  is the heat of fusion of pure PEO, which is equal to 213.7 Jg<sup>-1</sup> when, assumed as a 100% crystalline material, <sup>40</sup>  $\Delta H_m$  is heat of fusion of polymer blend electrolyte. The melting enthalpy of main matrix PVdF-HFP ( $\Delta H_{m2}$ ) also appreciably reduced when it is blended with PEO. The changes of thermal parameters in M-TiO<sub>2</sub> reinforced PEO/PVdF-HFP blend electrolyte is higher than U-TiO<sub>2</sub>/PEO/PVdF-HFP, which may due to organic functional groups like Si-O-Si, NH<sub>2</sub> and CH<sub>2</sub> may destroy the polymer chain confirmation and coordinate the salt systems. The new interactions formed by APS on TiO<sub>2</sub> not only interrupt structural confirmation of the polymer, but also provide a favorable conduction path for faster ion migration of I/I<sub>3</sub>. The relative percentage of crystallinity is significantly reduced with the addition of M-TiO<sub>2</sub> nanofillers than U-TiO<sub>2</sub> and it is corroborated with WAXD and FTIR in **Figure 1(c) and 2(e)**. The other thermal parameters and percentage of crystallinity derived from DSC were depicted in **Table. 1**

Table.1. Thermal parameters derived from DSC

Polymer Electrolyte	( $\Delta H_{m1}$ ) (J/g)	( $\Delta H_{m2}$ ) (J/g)	Glass Transition Temperature ( $^{\circ}\text{C}$ )	Crystallinity (%) (PEO)
PEO	109.1	-	-40.12	51.05
PVDF-HFP	-	24.70	-21.5	-
PEO/PVDF-HFP	49.32	22.96	-23.3	23.07
PEO/PVDF-HFP 7%U-TiO <sub>2</sub>	27.29	22.3	-23.8	12.70
PEO/PVDF-HFP 7%M-TiO <sub>2</sub>	26.53	10.33	-24.0	12.10

### 3.5. Dynamic Mechanical Analysis (DMA)

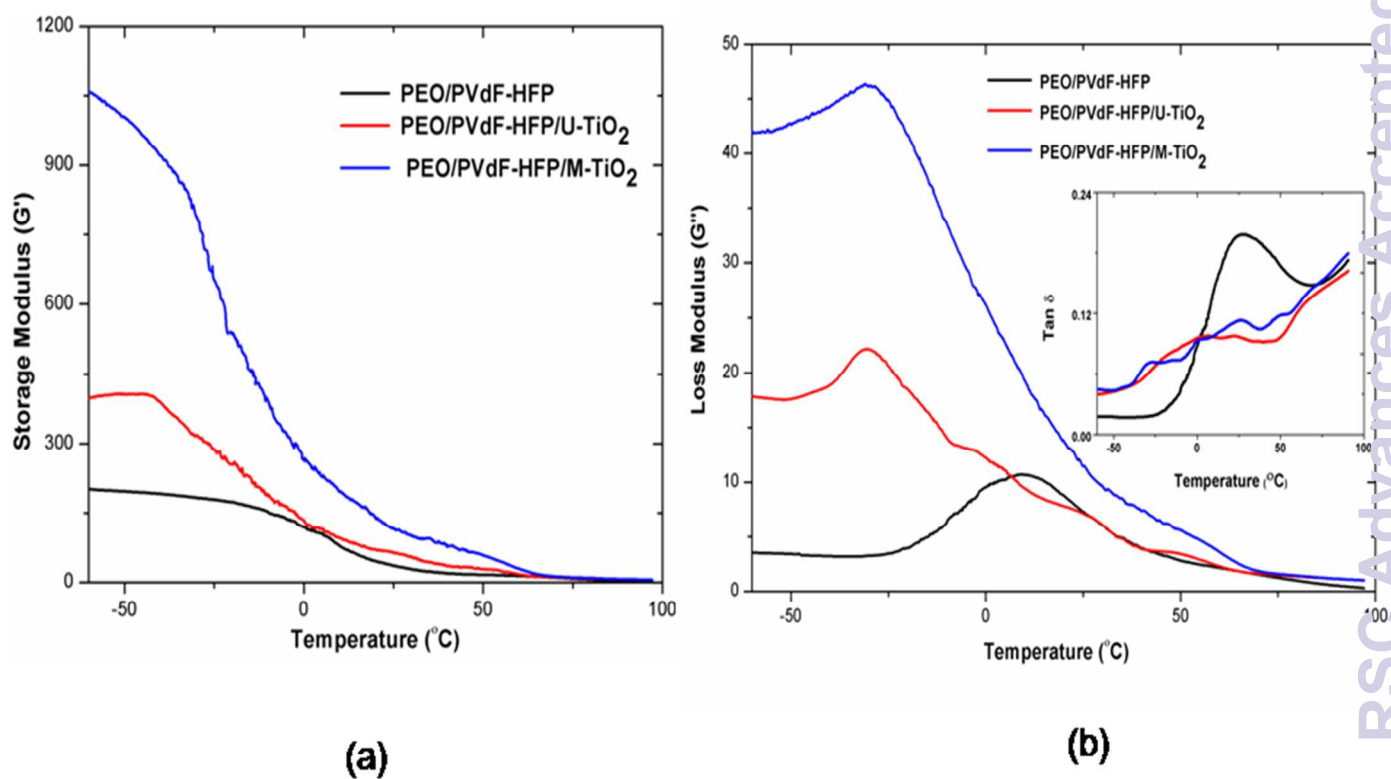


Fig. 4. DMA curves of PEO/PVDF-HFP blend and its blend nanocomposites electrolyte membranes (a) Storage modulus (b) loss modulus and tan delta (insert figure))

It is important to obtain membranes with high mechanical stability under dynamic conditions while developing polymer blend electrolytes for dye sensitized solar cells. DMA helps to study thermo mechanical property, polymer/polymer miscibility in polymer blend electrolytes and also measures the glass transition temperature of polymers. Fig.4. shows the variations of the storage modulus ( $E'$ ), the loss modulus and  $\tan \delta$  with the temperature for PEO/PVDF-HFP blend and its composite electrolytes. It is clear from Fig. 4(a) that storage modulus decreases with the increase of temperature for all blend electrolyte samples; however the decrease is not linear. The storage modulus curves of all samples exhibit three distinct region: a glassy high modulus region at low temperature where the segmental motion is restricted, a transition region where a substantial decrement takes place in  $E'$  with increase the temperature and a rubbery region where the drastic decay occurs in modulus values above the glass transition temperature. The storage modulus is increased in both glassy and rubbery region with the addition of U-TiO<sub>2</sub> and M-TiO<sub>2</sub>, moreover it is high value in glassy region than rubbery region as compared to PEO/PVDF-HFP electrolyte membrane.

The high storage modulus of PEO/PVDF-HFP blend nanocomposites at low temperatures is confirming the reinforcement effect of nanoparticles. It can be attributed to the restriction of the molecular motion of the PEO/PVDF-HFP blend macromolecules due to the fine dispersion of the nano-fillers is shown in AFM analysis **Fig. 3 (b)**, which leads to increased interactions with the polymer matrix.<sup>41</sup> The gradual decreasing trend of  $E'$  has been observed in between -40<sup>0</sup> C to 0°C, which is ascribed to glass transition temperature of PEO/PVDF-HFP blends.<sup>42</sup> It can be seen that the addition of nanoparticles has influence on the glass transition temperature of PEO/PVDF-HFP blend electrolyte.

A further abrupt decay in  $E'$  has been observed around 60°C with increase the temperature, undoubtedly it might be attributed to the melting characteristics of semicrystalline PEO component in the blend electrolytes. Even though the modulus is not completely vanished

nearby melting temperature of PEO, it is mainly contributed by the crystalline portion of the PVDF in the PVDF-HFP component.

**Fig.4 (b)** shows the plots of the loss modulus and loss tangent ( $\tan \delta$ ) (insert) as a function of temperature for PEO/PVDF-HFP blend and its nanocomposite electrolyte membranes. Generally, glass transition temperature of the polymeric materials is determined from the peak  $\tan \delta$  curves. But in present case it is difficult to distinguish  $T_g$  from its other relaxation peaks due to the movement of molecular chains at the amorphous-crystal interface of the semicrystalline polymers like PEO and PVDF-HFP.<sup>43</sup> It is not easy to find sharp glass transition ( $T_g$ ) from DMA curve due the presence of more heterogeneities in the PEO/PVDF-HFP composite electrolytes resulting in broader  $\tan \delta$  curve. And also the method of measurement plays very important role in determining the  $T_g$ . The rate of heating of samples was kept at 10°C per min, which may not be able to measure the micro-Brownian movement of molecular chains. Hence it is advisable to give the low heating rate for the determination of glass transition temperature in DMA analysis.

In other way, the glass transition temperature ( $T_g$ ) can be explained from the peak of loss modulus curve of polymer systems. It is clear that the loss modulus curve is showing a single peak which corresponds to the glass transition temperature, even though the peak has observed around 0°C for PEO/PVDF-HFP blend. But in the case of nanoparticles incorporated blend electrolytes exhibited a peak at lower temperature region and it is slightly decreased for M-TiO<sub>2</sub>. Hence, it is undoubtedly understood that incorporated nanofillers might be perturbed the crystalline domain and increase the free volume as well as flexibility of long range chain. Similar behavior of crystalline phase reduction is also observed in WAXD and DSC.

### 3.6. UV-VIS studies

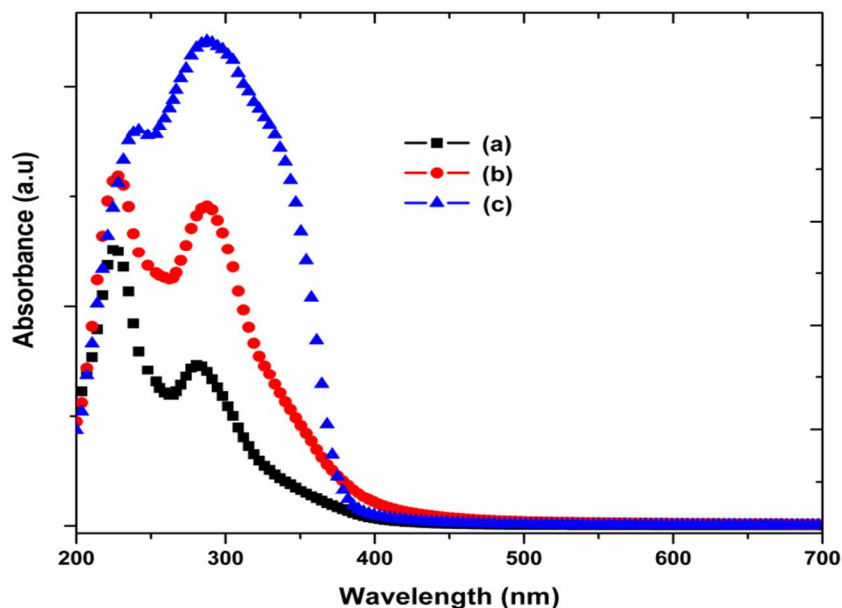


**Fig. 5. UV-vis spectra of (a) PEO/PVDF-HFP, (b) PEO/PVDF-HFP/U-TiO<sub>2</sub> and PEO/PVDF-HFP/M-TiO<sub>2</sub> composite electrolytes**

The UV-Vis absorption spectra of plasticized PEO/PVDF-HFP and U-TiO<sub>2</sub>, M-TiO<sub>2</sub> incorporated PEO/PVDF-HFP electrolyte membranes were shown in **Fig.5**. The peaks around 230 nm and 290 nm for all the samples are corresponding to I<sup>-</sup> and I<sub>3</sub><sup>-</sup> ions respectively. It is found that intensity of peaks was increased with the addition of TiO<sub>2</sub> nanoparticles. The nanoparticles in a polymer electrolyte play the role of Lewis acid base interaction centres with the ionic species in the electrolyte. The surface hydroxyl groups of the nanoparticles are expected to interact with the salt anions through the hydrogen bonds; hence the ion concentration has increased. But, in PEO/PVDF-HFP/ M-TiO<sub>2</sub> electrolyte membrane the high absorption peaks intensity is observed is shown in Fig.5 (c) indicates an increased free anion concentration (I<sup>-</sup> and I<sub>3</sub><sup>-</sup>). The peak point is slightly shifted to higher wavelength, which might be due to the interaction of silane molecules on TiO<sub>2</sub> surface. The similar interaction of free anions (I<sup>-</sup>/I<sub>3</sub><sup>-</sup>) with amine group (-NH) present in APS, have been observed from FTIR analysis by J.Zhang et al.<sup>44</sup> The

more free anions in the PVDF-HFP/M-TiO<sub>2</sub> electrolyte membranes are expected to enhance the ionic conductivity.

### 3.7. Electrochemical impedance studies

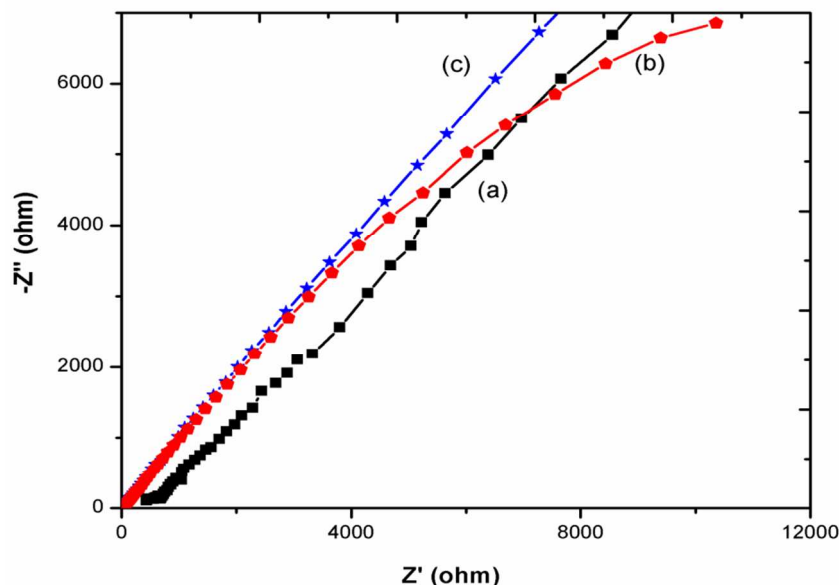


**Fig. 6. Nyquist plots of (a) PEO/PVDF-HFP (b) PEO/PVDF-HFP/M-TiO<sub>2</sub> and (c) PEO/PVDF-HFP/M-TiO<sub>2</sub> composite electrolytes**

The samples were optimized based on ionic conductivity measurements. The typical Nyquist plots of PVDF-HFP and its composite electrolyte membranes at room temperature are illustrated in **Fig. 6**. It was observed, the complex impedance spectra of electrolytes show only the slanted lines (spike) which indicates the electrode polarization plays the major role in the present polymer blend system. In practice the equivalent circuit model can help for the better understanding of the real system. Equivalent circuit for fitting the electrochemical impedance data shows in **Fig. s2†**, it is consisting of a serial combination of bulk electrolyte resistance ( $R_b$ ) and constant phase element (CPE).

The real and imaginary parts of impedance can be expressed as the following equations (2 and 3).<sup>45</sup>

$$Z' = R_b + \frac{\cos(\pi p/2)}{k^{-1}\omega^p} \quad \text{----- (2)}$$

$$Z'' = \frac{\cos(\pi p/2)}{k^{-1}\omega^p} \quad \text{----- (3)}$$

$Z'$  and  $Z''$  are the real and imaginary parts respectively,  $R_b$  is the bulk resistance of the blend electrolyte sample and  $k^{-1}$  corresponds to capacitance of constant phase element (CPE),  $\omega$  is angular frequency which is equal to  $2\pi f$  where  $f$  is the frequency in Hz and  $p$  is the fraction of right angle which the spike makes with the horizontal axis in Nyquist plot ( $Z''$  vs  $Z'$ ).

The complete linear behavior in the high frequency region of blend electrolytes is convincing evidence of the integrity of the system, which means the PEO/PVDF-HFP blend is miscible. If any phase separation and/or more crystallite domains have been exist, it would be exhibit the semicircles in the lower frequency region or, more generally, by deviation from linearity in the high frequency region of the impedance spectra.<sup>46</sup> It is understood that in **Fig. 6(a)** slight deviation of linear line at the lower frequency region in EIS spectra, indicates the high percentage of crystallinity of PEO/PVDF-HFP blend.

The electrical parameters such as diffusion coefficient ( $D$ ), ionic mobility ( $\mu$ ) and charge carrier density were calculated by using the following equations (4, 5 and 6) with the help of fitting parameters and plotted as a function of M-TiO<sub>2</sub> nanoparticles.<sup>45, 47</sup>

$$D = \frac{d^2}{\tau_2 \delta^2} \quad \text{----- (4)}$$

$$n = \frac{\sigma_{dc}}{e\mu} \quad \text{----- (5)}$$

$$\mu = \frac{eD}{kT} \quad \text{----- (6)}$$

Where  $d$  = thickness of sample/2,  $\delta = d/\lambda$ ,  $\lambda = \epsilon_0 \epsilon A/k^{-1}$  is the electrical double layer thickness,  $A$  is the area of electrolyte membrane,  $\epsilon_0$  is vacuum permittivity,  $\epsilon$  dielectric constant of polymer blend electrolytes  $\tau_2 = 1/\omega_2$ ,  $\omega_2$  is the angular frequency at which the spike interest at the real impedance axis. The intercept of the Nyquist plot ( $Z'$  vs  $Z''$ ) with the real axis at higher frequency region is taken as a bulk resistance ( $R_b$ ) of polymer electrolyte membranes. The ionic conductivity ( $\sigma$ ) of the electrolytes was calculated by using **Equation(7)**

$$\sigma = \frac{t}{R_b A} \quad \text{----- (7)}$$

Where,  $t$  is the thickness of the membrane,  $R_b$  is bulk resistance;  $A$  is the area of electrode in contact with electrolyte membrane.

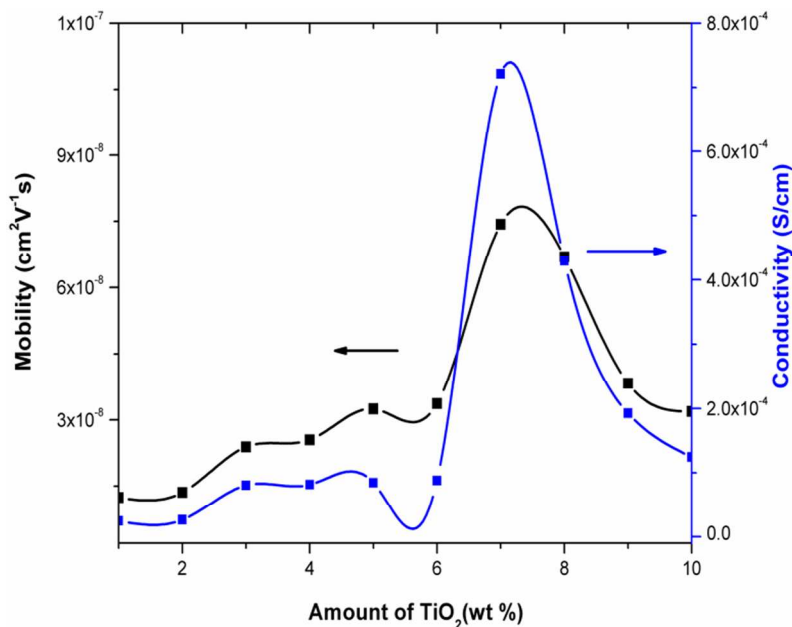


**Fig.7. Ionic conductivity and Ionic mobility of PEO/PVDF-HFP electrolyte membrane with different amount of silane treated TiO<sub>2</sub> nanoparticles**

**Fig.7.** Shows that the variation of ionic conductivity and mobility of ions in polymer blend nanocomposite electrolytes with inclusion of different amount of M-TiO<sub>2</sub>. The ionic conductivity increased by the addition of M-TiO<sub>2</sub> and exhibit maximum value of  $7.21 \times 10^{-4} \text{ Scm}^{-1}$  for 7 wt%. The nano range M-TiO<sub>2</sub> particles may influence the kinetics of high molecular weight polymer chain which promotes localized amorphous regions. Also, the addition of nanoparticles into polymer matrix give a three dimensional, mechanically stable and create a porous network structure. The anions (iodide/tri iodide) in the present electrolyte can easily move into the porous structures. For comparison purpose conductivity of 7 wt % of untreated TiO<sub>2</sub> incorporated PEO/PVDF-HFP composite also found about  $8 \times 10^{-5} \text{ S/cm}$  and it is lower than the same amount of silane modified TiO<sub>2</sub>. Further addition of M-TiO<sub>2</sub> exceeds the optimum level decreases the ionic conductivity of PEO/PVDF-HFP electrolytes due to the insulation of M-TiO<sub>2</sub> nanoparticles. Because, high concentration of nanoparticles also leads to well-defined crystallite regions and the added fillers beyond the optimum level may catalyze aggregation of polymer chains and thus increase the rate of recrystallization processes.<sup>47</sup> The more addition of nanofillers may cause to increase the viscosity of polymer blend electrolyte system; it hinders the ion mobility and dilution effect. The similar behavior has been observed for untreated nanoparticles incorporated polymer electrolytes.<sup>48</sup> These crystallite regions of polymer electrolytes restrict the movement of ions, thus ionic mobility also decreased beyond the optimum level of nano fillers. From these results, it clearly understood that the enhancement of the ion conducting property cannot be attributed to the electronic properties of semiconductor. Because, the interactions in polymer nanocomposite electrolytes are between salt-polymer, plasticizer-salt and the polymer-TiO<sub>2</sub> but not the salt-TiO<sub>2</sub> has investigated by Forsyth's et al.<sup>49</sup>

In the present study, it is mainly observed in WAXD studies (Fig.2. (e)) the disappearance of peaks and lowering of T<sub>g</sub> in DSC and DMA analysis (Fig.s1(e)†) and Fig.5) compared with unmodified counterpart. This is hinted that there may be an additional interaction

of  $\text{Li}^+$  in salt with nanoparticles in a surface modified  $\text{TiO}_2$  incorporated PEO/PVDF-HFP blend electrolyte system and the similar behavior also reported by Chin-Yeh Chiang et al.<sup>50</sup> supports our results. Such an additional interactions/coordination might be enhanced the ionic conductivity. The similar behavior has observed in silane modified PEO/PVDF blends by Y. Yang et al.<sup>44</sup> Because, the same amount of untreated nanoparticles incorporated PEO/PVDF-HFP electrolytes exhibits low ionic conductivity. The possible interaction of  $\text{Li}^+$  in salt with  $\text{TiO}_2$  in surface modified  $\text{TiO}_2$ /PVDF-HFP electrolyte system is sketched in **scheme. 2**

The diffusion coefficient and number of charge carriers within the blend electrolytes were derived and illustrated in **Fig. s3†**. It increased with the addition of M- $\text{TiO}_2$  nanoparticles within the PEO/PVDF-HFP blend electrolyte systems. The highest ionic diffusion coefficient has achieved for 7% incorporated M- $\text{TiO}_2$  electrolyte, beyond this level it decreased. The high filler content may be reduced the miscibility between PEO/PVDF-HFP and  $\text{TiO}_2$  nanoparticles; it leads to phase separation.<sup>49</sup> And also it can be increased the crystallinity of electrolytes, hence, it is believed to be an unfavorable environment for ion transport. The carrier concentration also decreased beyond the optimum level. The optimum amount of addition of M- $\text{TiO}_2$  (7 wt %) can dissociate/ coordinates the maximum number of  $\text{Li}^+$  and gives the maximum ionic conductivity. The dielectric constant is calculated and obtained maximum about 1260 for 8% of M- $\text{TiO}_2$  incorporated PEO/PVDF-HFP blends at 100 Hz. The decreasing trend of dielectric constant may be associated with exceeding of percolation threshold value. The electrical parameters of untreated  $\text{TiO}_2$  and surface modified  $\text{TiO}_2$  incorporated electrolyte was calculated and summarized in **Table. 2**

**Table 2. Calculated electrical parameter for 7% untreated TiO<sub>2</sub> incorporated PEO/PVDF-HFP**

PEO/PVDF-HFP With different amount of TiO <sub>2</sub>	Ionic conductivity $\sigma$ (S/cm) $\times 10^{-4}$	Mobility $\mu$ (cm <sup>2</sup> V <sup>-1</sup> s) $\times 10^{-8}$	No. of charge carriers $n$ (cm <sup>-3</sup> ) $\times 10^{22}$	Diffusion coefficient (cm <sup>2</sup> /s) $\times 10^{-10}$	Dielectric constant
1% M-TiO <sub>2</sub>	0.25	1.24	1.24	3.18	130
2% M-TiO <sub>2</sub>	0.26	1.35	1.21	3.45	170
3% M-TiO <sub>2</sub>	0.80	2.39	2.11	6.14	350
4% M-TiO <sub>2</sub>	0.81	2.55	1.99	6.55	420
5% M-TiO <sub>2</sub>	0.84	3.25	1.62	8.35	490
6% M-TiO <sub>2</sub>	0.88	3.37	1.63	8.66	550
*7% M-TiO <sub>2</sub>	7.24	7.43	4.41	19.11	1020
8% M-TiO <sub>2</sub>	4.29	6.69	4.01	17.20	1260
9% M-TiO <sub>2</sub>	1.93	3.83	3.14	9.85	987
10% M-TiO <sub>2</sub>	1.25	3.19	2.43	8.21	927
*7% U-TiO <sub>2</sub>	0.26	1.35	1.21	3.45	172

\* Optimized compositions

### 3.8. Thermo gravimetric Analysis (TGA)

TGA and DTA curves of PEO/PVDF-HFP and its nanocomposite electrolyte membranes were shown in **Fig. s4†**. It is observed that the stability of all samples blends slightly moves down at lower temperature around 50° C with a weight loss of 8-10 %. It is well known that the evaporation of moisture and physically absorbed silane molecule attached on the PEO and TiO<sub>2</sub> surface. It is seen for PEO/PVDF-HFP blends, no significant weight loss was observed until 240°C followed by weight loss DTA exothermic peak which is clearly showed that PEO/PVDF-HFP blend system is stable upto 370°C. The majority of weight loss started around 400°C, this

may be due to thermal degradation of random chain scission of C–O bonds in PEO.<sup>51</sup> The main degradation products are ethyl alcohol, methyl alcohol, alkenes, non-cyclic ethers (ethoxymethane, ethoxyethane and methoxymethane), formaldehyde, acetic aldehyde, ethylene oxide, water, CO and CO<sub>2</sub>.<sup>52</sup> Beyond this temperature the thermal stability of the membranes is due to the repeating units  $-(CF_2-CF_2)-$  of PVDF-HFP. The chemical bond strength of C-F is approximately 485kJ/mol, which is higher than C-H and C-C bond strengths around 435kJ/mol and 410 kJ/mol respectively.<sup>53</sup> Further increasing temperature, the stability of nanocomposites films increased due to TiO<sub>2</sub> nanoparticles. In present case, the thermal stability composite electrolyte at high operating temperature is not required for practical applications of DSSC.

### 3.9. Cyclic Voltammetry Analysis of MWCNT/ Nafion<sup>®</sup>

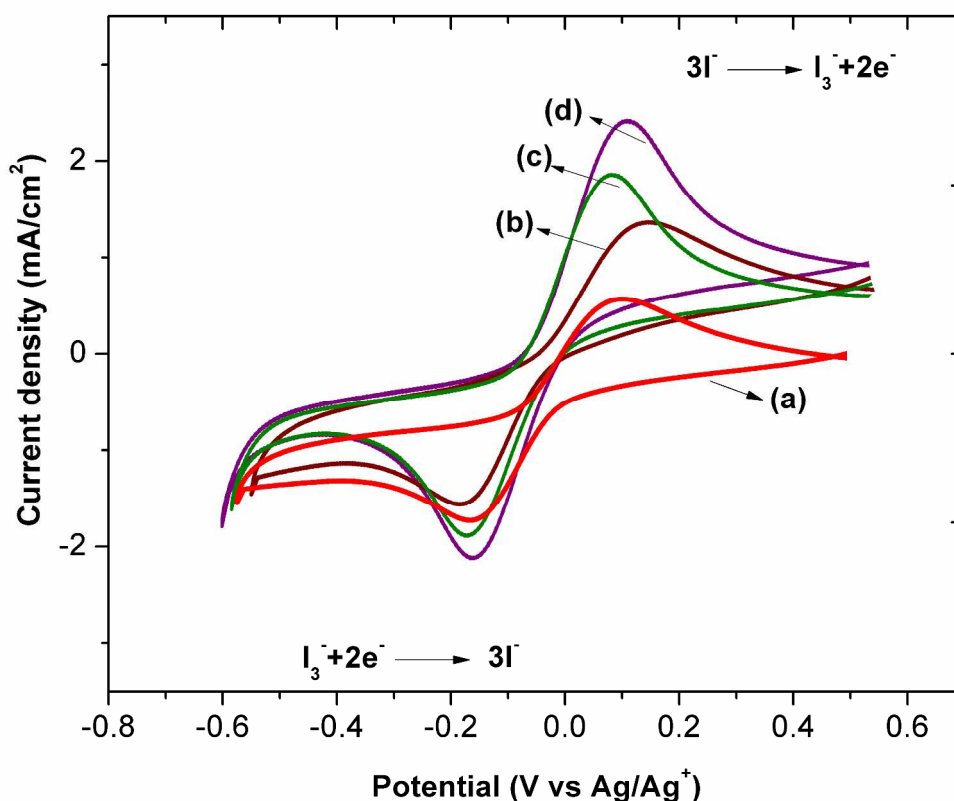


**Fig.8.** Cyclic voltammety studies of MWCNT/ Nafion<sup>®</sup> composite: MWCNT: (a) 0.5, (b) 1, (c) 1.5 and (d) 2 wt %).

To investigate the electro catalytic activity of MWCNT /Nafion<sup>®</sup> composite for I<sub>3</sub><sup>-</sup> reduction at the electrode was employed in cyclic voltametry technique. **Fig.8.** shows that typical CV characteristics curve of MWCNT/Nafion<sup>®</sup> composite electrode with different amount of MWCNT at a scan rate of 10 mVs<sup>-1</sup>. The catalytic activity is increased with increase the amount of MWCNT and reaches maximum for 2 wt% (Fig.8(d)). For comparison purpose Pt electrode is taken as reference electrode and performed at the same conditions is depicted in **Fig.s5.†**. The peak position and shape of the curve for MWCNT/Nafion<sup>®</sup> are almost similar to the Pt electrode. The cathodic peak at -0.167 V with the peak current (I<sub>c</sub>) of -2.21 mA/cm<sup>2</sup> assigned to the redox reaction is given equation (8) I<sub>3</sub><sup>-</sup>/I<sub>3</sub><sup>-</sup>.



The anodic peak at 0.13V with the peaks current of 2.67 mA/cm<sup>2</sup> is assigned to the redox reaction is given in equation (9)



The peak current density of MWCNT (2 wt%) is quit comparable with the Pt coated electrodes (**Fig.s5.†**). It is mainly due to the uniform distribution MWCNT caused by Nafion<sup>®</sup> in the coating solution, which inhibits the aggregation in coated films. Hence, high electrochemically active surface area of MWCNT/Nafion<sup>®</sup> composite can be improved the electro catalytic activity. This indicates the carbon based nanoparticles can be utilized as an alternative candidate to replace the precious metals as counter electrodes. The similar work had reported by Min-Hsin Yeh et al with Graphene/Nafion<sup>®</sup> nanocomposites as a counter electrode for DSSC applications.

54

### 3.10. Photovoltaic Performance of SSDSSC

J-V characteristics curves of PEO/PVDF-HFP and blend nanocomposite based DSSC were shown in **Fig. 9**.

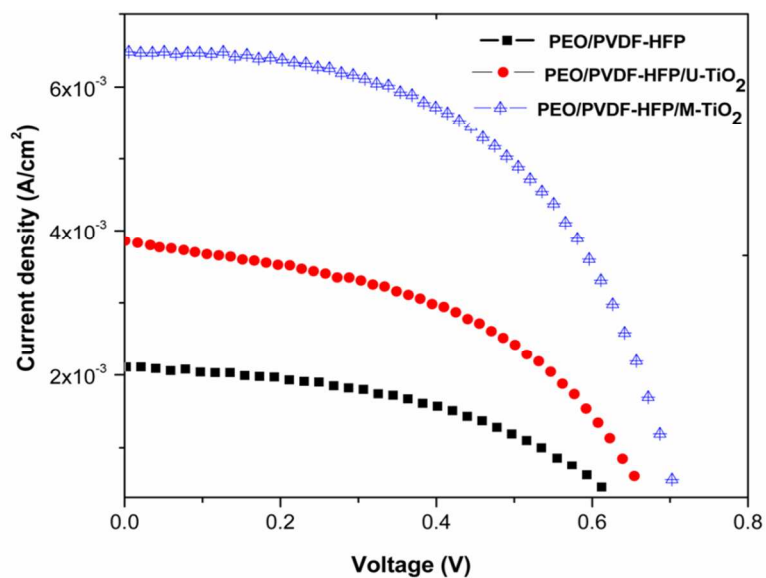


**Fig.9. J-V characteristics curves SSDSSC PEO/PVDF-HFP and its composite electrolytes**

**Table.3.** shows that the photovoltaic parameters of SSDSSC derived from J-V curve. It observed that, the addition of U-TiO<sub>2</sub> and M-TiO<sub>2</sub> nanoparticles within the PEO/PVDF-HFP blend, photo-current density ( $J_{\max}$ ) has increased from 1.26 mA/cm<sup>2</sup> to 2.77 mA/cm<sup>2</sup>, 5.36 mA/cm<sup>2</sup> respectively. It is well known that the performance of DSSC is mainly determined by effective transport behaviour of I<sup>-</sup> and I<sub>3</sub><sup>-</sup> ions. The high concentration of I<sup>-</sup> and I<sub>3</sub><sup>-</sup> ions is shown in UV-Vis (**Fig. 5 (c)**) spectra may cause to increase the ionic conductivity and favours to achieve the high  $J_{\text{sc}}$  and  $V_{\text{oc}}$  for M-TiO<sub>2</sub> incorporated PEO/PVDF-HFP blend nanocomposites. The improvement in the efficiency and fill factor for PEO/PVDF-HFP/ M-TiO<sub>2</sub> electrolyte is mainly due to the reduction in the crystallinity followed by increasing ionic conductivity to about  $7.21 \times 10^{-4}$  S/cm. The more amorphous phase of PEO/PVDF-HFP/ M-TiO<sub>2</sub> electrolyte can provide easy migration of ions from electrolyte to electrode. This can help to regenerate the dye molecules from its oxidized states (D<sup>+</sup>) to normal state (D). These are the main factors for improved the performances. The APS molecules on TiO<sub>2</sub> surface in PEO/PVDF-HFP electrolyte not only

increases the ionic conductivity but also inhibits the charge recombination of conduction band electrons of dye sensitized TiO<sub>2</sub> and I<sub>3</sub><sup>-</sup>. Hence, it is beneficial for the enhancement of V<sub>oc</sub>.

**Table 3. Photovoltaic parameters for PVDF-HFP and its blend nanocomposite electrolytes**

Polymer Electrolytes	V <sub>oc</sub> V	J <sub>sc</sub> mA/cm <sup>2</sup>	V <sub>max</sub> V	J <sub>max</sub> mA/cm <sup>2</sup>	F.F (%)	Efficiency %	References
PEO/PVDF-HFP	0.62	2.13	0.45	1.26	43	0.6	present
PEO/PVDF-HFP/U-TiO <sub>2</sub>	0.67	3.85	0.50	2.77	54	1.4	present
PEO/PVDF-HFP/M-TiO <sub>2</sub>	0.71	6.37	0.53	5.36	62	2.8	present
TiO <sub>2</sub> nanotube (TNT)/PEO electrolyte	0.37	0.58	0.29	0.43	58	0.124	[63]
PEO/PVDF	0.61	7.2	-	-	77	3.38	[65]

Generally, the high efficient (efficiency,  $\eta > 3\%$ ) DSSCs are employing liquid electrolytes, plasticizers, other toxic materials like 4-tertbutyl pyridine and iso-cyanate compounds as additives.<sup>55-59</sup> However, the efficiency ( $\eta=2.8\%$ ) in the present work is quite comparable with recently reported efficiency ( $\eta$ , 2% -5%).<sup>60-62</sup> In another way it is interesting to note that the efficiency of ZnO photo anode based DSSCs are higher than TiO<sub>2</sub> as a photo anode material. Because, the thickness of the ZnO based photo anode is higher than TiO<sub>2</sub> Photo anode sintered at 400° C.<sup>64</sup> Hence, the amount of dye absorption by TiO<sub>2</sub> is very less and its high grain boundary resistance leads to impede the electrons emitted from dye. These factors also cause to affect the photovoltaic performance of DSSCs. Currently; we are optimizing the photo anode materials with the combinations of TiO<sub>2</sub>, ZnO and Fe<sub>2</sub>O<sub>3</sub> by changing the composition, morphology and particle size which will be discussed in the near future.

However, our main concern is here, whether the surface modified  $\text{TiO}_2$  can improve the conversion efficiency of DSSC as compared with PEO/PVDF-HFP/ $\text{U-TiO}_2$  electrolyte system. The above results exposed that of surface modification of  $\text{TiO}_2$  nanoparticles within polymer electrolytes is an effective approach for solid state DSSC applications than other expensive organic additives.

### 3.11. Internal resistance of DSSC

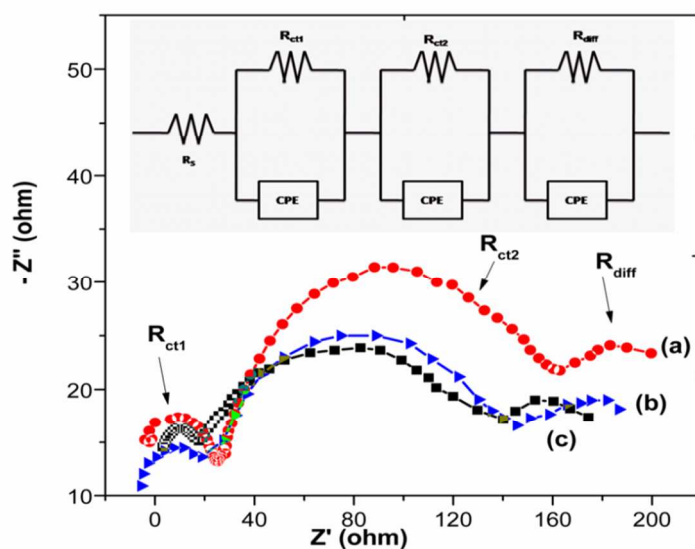


**Figure. 10.** EIS spectra of DSSC with different electrolytes (a) PEO/PVDF-HFP (b) PEO/PVDF-HFP/ $\text{U-TiO}_2$  and (c) PEO/PVDF-HFP/ $\text{M-TiO}_2$

The internal resistance of various interfaces in DSSC was measured by electrochemical impedance spectroscopy (EIS). In Fig.10.shows that EIS spectra of DSSC based on PEO/PVDF-HFP and its composites electrolytes. It is seen that three distinct semi-circles observed in the frequency range of  $10^{-3}$  Hz  $-10^6$  Hz. These semicircles are due to Nernst diffusion within the electrolyte, the electron transfer at the  $\text{TiO}_2$ /electrolyte interface and the redox reaction at the

MWCNT/Nafion<sup>®</sup> counter electrode. The experimental EIS data fitted with equivalent circuit and charge transfer resistance of each interface have derived.

$R_s$  is denoted as the series resistance of the electrolytes and electric contacts in the DSSCs. And  $R_{ct1}$ ,  $R_{ct2}$  and  $R_{diff}$  correspond to the charge transfer process occurring at the MWCNT/Nafion<sup>®</sup> counter electrode/electrolyte (corresponding to the first arc), the FTO/TiO<sub>2</sub>/electrolyte interface (corresponding to the second arc) and the Warburg element of the ionic diffusion for the redox-couple (I/I<sub>3</sub><sup>-</sup>) ion diffusion in the electrolyte (third arc) respectively.

<sup>66-68</sup> The EIS parameters were summarized in **Table. s1.†**.

From, the **Table. s1.†** DSSC based on PEO/PVDF-HFP/M-TiO<sub>2</sub> electrolyte shows smaller  $R_{ct2}$  and  $R_{diff}$  than pure and U-TiO<sub>2</sub> incorporated. It is attributed to the uniform distribution of M-TiO<sub>2</sub> within the matrix and reduced crystallinity of PEO/PVDF-HFP can be facilitated the ion diffusion coefficient (I/I<sub>3</sub><sup>-</sup>). Hence, the photocurrent and solar energy conversion efficiency of PEO/PVDF-HFP/M-TiO<sub>2</sub> based DSSC were marginally increased.

#### 4. Conclusions

In summary, PEO/PVDF-HFP blend electrolyte membranes reinforced with surface modified TiO<sub>2</sub> nanofiller were prepared for dye sensitized solar cell applications. The Electrochemical studies revealed that the addition of surface modified nanoparticles increased the ionic conductivity up to  $7.21 \times 10^{-4}$  S/cm for 7 wt%, which is almost 10 times higher than the unmodified counterpart within PEO/PVDF-HFP blend. The ionic mobility, charge carrier concentration and ion diffusion coefficient are also found to increase with the incorporation of surface modified TiO<sub>2</sub> nanoparticles. The influence of the TiO<sub>2</sub> nanoparticles surface functionality upon the degree of crystallinity of the polymer matrix was analyzed using DSC and WAXD, it is observed that amorphous phase is increased. Thermo mechanical behavior of the composite membranes also confirmed that reduction in crystallinity. The thermo gravimetric

investigations of membranes indicated the thermal stability of blend improved upon the addition of nanosized inorganic fillers. The surface morphology of electrolyte membranes was studied by AFM. The solid state dye sensitized solar cell was fabricated by using silane modified  $\text{TiO}_2$ /PEO/PVDF-HFP polymer nanocomposites electrolyte, MWCNT/Nafion<sup>®</sup> as counter electrode and N-719 as a sensitizer. The maximum solar conversion efficiency of 2.84% was achieved with silane modified  $\text{TiO}_2$  incorporated electrolyte. The addition of surface modified  $\text{TiO}_2$  within the electrolytes also decreases the interfacial resistance. These results, confirmed the active role of silane modification of  $\text{TiO}_2$  which leads to increase in transport properties and photo-current conversion efficiency.

#### **Acknowledgement**

One of the authors K.Prabakaran is thankful to Prof. P. Ramasamy and Dr. M. Senthil Pandian, SSN Research Centre, Chennai, Tamilnadu for their support in Photo anode fabrications and characterizations. This research received no specific grant from any funding agency.

## REFERENCES

1. J.Liu, Y. Zhao, A.Weil, Z. Liu, F. Luo J Mater Sci: Mater Electron., 2014 **25**, 4008.
2. M. Marandi, S. Feshki M.N. S. Sabet, Z. Anajafi and N. Taghavinia, RSC Adv., 2014,**4**, 58064.
3. A. Yella, H.W. Lee, H.N. Tsao, C. Yi, A.K. Chandiran, M. Nazeeruddin, E.W. Diau, C.Y. Yeh, S.M. Zakeeruddin, M. Gratzel, Science, 2011, **334**, 629.
4. R.H.Lee, J. K.Liu, J.H.Ho, J.W. Chang, B.T.Liu, H.J.Wang, R.J. Jeng, polymer Int. 2011, **60**, 483.
5. H. Sakamoto, S. Igarashi, K. Niime, M. Nagai, Organic Electronics 2011, 12, 1247.
6. R. Kawano , T. Katakabe , H. Shimosawa , M. K. Nazeeruddin, M.Grätzel , H. Matsui , T. Kitamura , N. Tanabe and M.Watanabe, Phys. Chem. Chem. Phys., 2010, **12**, 1916.
7. P. Wang, S. M. Zakeeruddin, J.E. Moser, M.K. Nazeeruddin, T. Sekiguchi, M. Grätzel, Nature Materials, 2003, **2**, 402.
8. J.Wu, S. Hao, Z. Lan, J. Lin, M. Huang, Y. Huang, P. Li, S. Yin and T. Sato An, J. Am. Chem. Soc.2008, **130**, 11568.
9. X. Li, Y. Zhao, L. Cheng, M. Yan, X. Zheng, Z. Gao, Z. Jiang, Journal of Solid State Electrochemistry, 2005, **9**, 609.
10. S. Yoon, K. Ichikawa , W.J. MacKnight , S. L. Hsu, Macromolecules, 1995, **28**, 4278.
11. K. W. Chew, and K. W. Tan, Int. J. Electrochem. Sci., 2011, **6**, 5792.
12. X. G. Zhao, J.Y. Park, H-B. Gu, Journal of The Electrochemical Society, 2014, **161** (9) H517.
13. D. Saikia , C.C. Han, Y.W. Chen-Yang Journal of Power Sources, 2008, **185**, 570.

14. N. Angulakshmi, S. Thomas, K. S. Nahm, A. Manuel Stephan, R. Nimma Elizabeth, *Ionics*, 2011, **17**, 407.
15. R. Prasanth, N. Shubha, H. H. Hng, M. Srinivasan, *Journal of Power Sources*, 2014, **245**, 283.
16. Z. Huo, S. Dai, K. Wang, F. Kong, C. Zhang, X. Pan and X. Fang, *Energy Mater. Sol. Cells*, 2007, **91**, 1959.
17. P. K. Singh, B. Bhattacharya, R. K. Nagarle, *Journal of Applied Polymer Science*, 2010, **118**, 2976.
18. Y. Zhau, W. Xiang, S.Chen, S. Fang, X.Zhou, J. Zhang, Y.Lin, *Chem. Com.*, 2009, **26**, 3895.
19. J.Zhang, H. Han, S.Wu, S.Xu, Y.Yang, C. Zhou, X. Zhao, *solid state ionics*, 2007, **178**, 1595.
20. Niparat Tiautit, Chonnipa Puratane, Sanit Panpinit, and Sayant Saengsuwan *Energy Procedia*, 2014, **56**, 378.
21. Y. Fang , J. Zhang , X. Zhou , Y. Lin, S. Fang, *Electrochemistry Communications*, 2012 **16**, 10.
22. M. Sivakumar. R.Subadevi, R. Muthu pradeepa, *AIP Conference Proceedings*, 2013, **1536**, 857.
23. H. Chae, D. Song, Y. G. Lee, T. Son, W. Cho, Y. B. Pyun, T. Y. Kim, J.H. Lee, F. F. Santiago, J. Bisquert, and Y.S.Kang, *Journal of Phys. Chem. C*, 2014, **118 (30)**, 16510.
24. M. Sethupathy, S. Ravichandran, P. Manisankar, *Int. J. Electrochem. Sci.*, 2014, **9**, 3160126.
25. N. Jeon, D.W. Kim, *Journal of Nanosci. Nanotechnology*, 2013, **13**, 7955.
26. L. Xie, X. Huang, K. Yang, S. Li, P. Jiang, *J. Mater. Chem. A*, 2014, **2**, 5244.

27. K. Prabakaran, S. Mohanty, S. K. Nayak *Journal of Materials Science: Materials in Electronics*, 2014, **25**, 4590.
28. S.M. Mirabedini, M. Sabzi, J. Zohuriaan-Mehr, M. Atai, M. Behzadnasab, *Applied Surface Science* 2011, **F**, 4196
29. Y. Yang, J. Zhang, C. Zhou, J. Wu, S. Xu, W. Liu, H. Han, B. Chen, X.Z. Zhao, J. *Phys.Chem. B*, 2008, **112**, 6594.
30. M. Deka, A. Kumar *Bull. Mater. Sci.*, 2009, **32**, 627.
31. S. Rajendran, O. Mahendran, R. Kanan, *Mater. Chem. Phys.*, 2002, **74**, 52.
32. D. Saikia, A. Kumar, *ElectrochimicaActa*, 2004, **49**, 2581.
33. K. Pandey, M. M. Dwivedi, N. Asthana, M. Singh, S. L. Agrawal, *Materials Sciences and Application*, 2011, **2**, 721.
34. Y. Y. Hao, J. Peng, W. Furong, W. Lefu, L. Xuehui, *Science China Chemistry*, 2012, **55**, 1608.
35. Y. Liu, J.Y. Lee, L. Hong, *Solid State Ionics*, 2002, **150**, 317.
36. S. Abbrent, J. Plestil, D. Hlavata, J. Lindgren, J. Tegenfeldt, A. Wendsjo, *Polymer*, 2007, **42**, 1407.
37. X.D. Ma, X.F. Qian, J. Yin, Z.K. Zhu, *Journal of Materials Chemistry*, 2002, **12**, 663.
38. J. Zhang, Y. Yang, S. Wu, S. Xu, C. Zhou, H. Hu, B. Chen, X. Xiong, B. Sebo, H. Han and X. Zhao, *Nanotechnology*, 2008, **19**, 245202.
39. L.F. Malmonge, J. A. Malmonge, W. K. Sakamoto, *Materials Research*, 2003, **6**, 469.
40. A.M.M.A. Ali, R.H.Y. Subban, H. Bahron, T. Winnie, F. Latif, M.Z.A. Yahya, *Ionics*, 2008, **14**, 491.
41. D.N. Bikiaris, N.P. Nianias, E. G. Karagiannidou, A. Docoslis, *Polymer Degradation and Stability*, 2012, **97**, 2077.
42. C. Komalan, K. E. George, P. A. S. Kumar, K. T. Varughese, S. Thomas, *eXPRESS Polymer Letters*, 2007, **10**, 641.

43. V.J. McBrierty, D.C.Douglass, T.A..Weber Polym Sci Polym Phys Ed., 1976, **14**, 1271.
44. J.Zhang, Y.Yang, S. Wu, S. Xu, C. Zhou, H. Hu, B. Chen, H. Han, X. Hao, *Electrochimica Acta*, 2008, **53**, 5415.
45. A.K.Arof, M.Naeem, F.Hameed, W.J.M.S.R.Jayasundara, M.A.Careem, L.P.Teo, M.H. Buraidah, *Optical and quantum electronics*, 2014, **46**,143.
46. W.A.Van Schalkwijk and B. Scrosati (Eds), ‘Advances in Lithium Ion Batteries’ (Kluwer Academic/Plenum Publishers, New York, 2002.
47. S.Ramesh, K.Ramesh and A.K.Arof Int., *J. Electrochem. Sci.*, 2013, **8**, 8348.
48. Z. Changneng, W. Miao, Z. Xiaowen, L. Yuan, F. Shibi, L. Xueping, X. Xuri & C. Kuang, *Chinese Science Bulletin*, 2004, **49**, 2033.
49. M. Forsyth, D.R. MacFarlane, A. Best, J. Adebahr, P. Jacobsson, A.J. Hill, *Solid State Ionics*, 2002, **147**, 203.
50. C. Y. Chiang, M. Jaipal Reddy, Peter P. Chu, *Solid State Ionics*, 2004, **175**, 631.
51. P. S.Claire *Macromolecules*,2009, **42**, 3469.
52. M. Jaki, N. S. Vrandeci, I. Klari, *Polymer Degradation and Stability* 2013, **98**, 1738.
53. S. Ramesh, Ong Poh Ling, *Polym. Chem.*,2010, **1**, 702.
54. M-H. Yeh, C-L. Sun, J-S. Su, L-Y. Lin, C-P. Lee, C-Y. Chen, C-G. Wu, R. Vittal, K-C. Ho, *Carbon*, 2012, **50**, 4192.
55. Z.Lan , J. Wu, J. Lin, M.Huang, S. Yin, T. Sato, *Electrochimica Acta*, 2007, **52**, 6673.
56. A.K. Arof , H.K. Jun, L.N. Sim, M.Z. Kufian, B. Sahraoui *Optical Materials*, 2014, **36** 135.
57. S. P. Lim, A.Pandikumar, N.M. Huang and H. N. Lim, *RSC Adv.*,2014, **4**, 38111.
58. L. Yu, W. Shi, L. Lin, Y. Liu, R. Li, T. Peng and X. Li *Dalton Trans.*, 2014,**43**, 8421.
59. L. Wei, Y. Yang, R. Fan, P. Wang, L. Li, J. Yu, B.Yang and W. Cao, *RSC Adv.*, 2013,**3**, 25908.

60. T. M. W. J. Bandara, W. J. M. J. S. R. Jayasundara, M. A. K. L. Dissanayake, I. Albinsson, B.E. Mellander *Phys. Chem. Chem. Phys.*, 2012, **14**, 8620.
61. X. Zhang, J. Liu, S. Li, X. Tan, M. Yu and J. Du, *RSC Adv.*, 2013, **3**, 18587.
62. U. Nithiyantham, R. Ananthakumar and S. Kundu, *RSC Adv.*, 2014, **4**, 35659.
63. S. Suresh, A. Pandikumar, S. Murugesan, R. Ramaraj, S. Paul Raj. *Solar Energy*, 2011, **85**, 1787.
64. Y. Horiguchi, K. Kinoshita, K. Hara, K. Sayama, and S. Arakawa, *The Advanced Materials and Opto-Electronics (Technical Report)*; Simitomo Osaka Cement Co. Ltd., Japan, 2001, p. 18.
65. L. Wei, Y. Yang, R. Fan, P. Wang, L. Li, J. Yu, B. Yang, W. Cao, *RSC Adv.*, 2013, **3**, 25908.
66. Y. Rong, Z. Ku, M. Xu, G. Liu, H. Wang, H. Han, *Proc. of SPIE* 2013, **8830** 88301W-2, DOI: 10.1117/12.2023774.
67. J. Lim, M. Lee, B. Suresh Kannan, J. Kim, D. Kim, Y. Jun *RSC Advances*, 2013, **3**, 4801
68. X.G. Zhao, E. M. Jin, J-Y. Park, H-B. Gu *Composites Science and Technology*, 2014, **103**, 100.

